Eurasian Journal of Physics and Functional Materials

2026, 10(3), 210-218

The effect of Nb doping on the structural and chemical properties of MoS_2

R.K. Daurenbekova[1,*], A. Zhussupbekova[2,3,4], A. Cabero del Hierro[2], D.H. Daurenbekov[1], I.V. Shvets[2,4], K. Zhussupbekov[2,4,5]

[1]Institute of Physical and Technical Sciences, L.N. Gumilyov Eurasian National University, Astana, Kazakhstan

[2]School of Physics, Trinity College Dublin, The University of Dublin, Dublin, Ireland

[3]School of Physical Sciences, Dublin City University, Dublin, Ireland

[4]Centre for Research on Adaptive Nanostructures and Nanodevices (CRANN), Trinity College Dublin, Dublin, Ireland

[5]Department of Physics, Harvard University, Cambridge, Massachusetts, USA

E-mail: daurenbekova_rk@enu.kz

DOI: **10.32523/ejpfm.2026100301**
Received: 15.07.2026 - after revision

Substitutional doping is one of the principal approaches used to control the electronic properties of layered transition-metal dichalcogenides. In this work, pristine and Nb-doped MoS_2 were comparatively investigated using low-energy electron diffraction, X-ray photoelectron spectroscopy, including valence-band measurements, and Raman spectroscopy. The LEED patterns show that the Nb-doped sample retains the characteristic hexagonal surface structure of MoS_2, although the enhanced diffuse background and additional weak diffraction features indicate an increased degree of structural disorder or the presence of additional surface domains. Core-level XPS spectra confirm that the dominant Mo^{4+} – S^{2-} chemical environment characteristic of MoS_2 is preserved, with no evidence of substantial surface oxidation or secondary sulfur-containing phases. The Nb 3d signal was not directly resolved, consistent with the low nominal dopant concentration and the sensitivity limits of the XPS configuration employed. However, correlated shifts of the valence-band, Mo 3d, and S 2p features towards lower binding energy indicate an Nb-induced modification of the electronic structure, consistent with acceptor-type Nb incorporation into the MoS_2 host lattice. The Raman spectra of both samples exhibit the characteristic E^1_{2g} and A_{1g} modes, confirming that the vibrational structure of 2H- MoS_2 is retained after doping. Overall, low-level Nb doping modifies the electronic structure and increases structural disorder without causing large-scale disruption or phase transformation of the MoS_2 matrix.

Keywords: MoS_2; Nb doping; LEED; XPS; Raman spectroscopy; surface structure; chemical state

Introduction

Two-dimensional (2D) materials have attracted considerable attention since the discovery of graphene [1, 2]. This interest is driven by both fundamental scientific questions [3, 4], and the prospects for practical applications [5, 6]. Among 2D materials, transition-metal dichalcogenides (TMDs) have been particularly widely investigated. Their general chemical formula is MX_2, where M is a transition metal, such as Mo, W, or Pt, and X is a chalcogen, such as S, Se, or Te. This work focuses on MoS_2 [7–9], one of the most extensively studied members of the TMD family.

MoS_2 is of particular interest because its electronic properties strongly depend on its thickness. Several theoretical and experimental studies have shown that bulk MoS_2 has a band gap of approximately 1.2 eV, whereas the band gap of monolayer MoS_2 increases to approximately 1.9 eV [7, 10, 11]. This tunable band gap has stimulated research into applications in multilevel data storage [12], optoelectronic devices [13], electrocatalysis [14], and diodes [15].

The electronic and mechanical properties of 2D materials can be substantially altered by individual defects, adsorbed species, and substitutional dopants [16–20]. Defect engineering is therefore an important strategy for tailoring material properties [21], but it requires a detailed understanding of how defects influence the local atomic and electronic structure. Defects may originate from the substrate, environmental exposure, or the synthesis process and may occur as vacancies, interstitial atoms, substitutional impurities, or more complex defect configurations. Such defects can create surface states and significantly modify local electronic properties [22–26], which may be either beneficial or undesirable depending on the intended application. Although intrinsic point defects in pristine TMDs have been studied extensively [26–31], p- and n-type-doped Mo-based TMDs remain less well understood at the atomic scale, and many studies in this area rely primarily on computational modelling.

Controlled p- and n-type doping of MoS_2 is of considerable interest because it enables modification of the charge-carrier concentration and the associated electronic properties of the material. In particular, Nb is regarded as a promising acceptor-type dopant when it substitutes for Mo atoms. However, dopant incorporation may also affect structural order, the chemical state of the surface, and the vibrational properties of the lattice. A comparative characterisation of pristine and Nb-doped MoS_2 is therefore necessary to determine whether the structure of the host matrix is preserved after doping. However, a direct comparison of the surface crystallographic order of pristine and low-concentration Nb-doped bulk MoS_2 by LEED, combined with XPS and Raman spectroscopy, remains limited.

Materials and methods

Pristine and Nb-doped MoS_2 single crystals were purchased from HQ Graphene. Pristine and Nb-doped MoS_2 samples were investigated using low-energy electron diffraction (LEED), X-ray photoelectron spectroscopy (XPS), and Raman

spectroscopy. The combined application of these techniques enabled evaluation of the surface crystallographic order, the chemical states of the constituent elements, and the vibrational properties of the lattice. The measurements were used to assess comparatively the effect of low-level Nb doping on the structural and chemical properties of MoS_2.

The pristine and Nb-doped MoS_2 samples were cleaved in situ using adhesive tape in the preparation chamber at a pressure of approximately 5×10^{-7} mbar. Immediately after cleavage, the samples were transferred without exposure to the atmosphere into the analytical chamber, which had a base pressure below 5×10^{-11} mbar.

LEED measurements were performed directly after cleavage to examine the surface symmetry and long-range crystallographic order. Diffraction patterns from the pristine and Nb-doped MoS_2 samples were recorded at a primary electron energy of 93 eV. The measurements were used to compare the degree of surface order and diffuse scattering in the two samples. A similar UHV-based approach combining LEED and XPS has previously been used to assess the order and chemical cleanliness of freshly prepared surfaces.

XPS measurements were performed using monochromated Al Kα radiation with a photon energy of 1486.7 eV. Survey spectra and high-resolution spectra of the Mo 3d/S 2s and S 2p regions were acquired to determine the chemical states of Mo and S, assess the presence of surface oxidation, and examine whether an Nb-related signal could be detected. Comparable measurements were carried out using an Omicron MultiProbe XPS system with an instrumental resolution of approximately 0.6 eV and a base pressure of 5×10^{-11} mbar. The binding-energy scale was referenced to the analyzer Fermi level, and both samples were electrically grounded during acquisition.

Raman spectra were collected using a WITec Alpha 300 R system with a 532 nm excitation laser. Measurements were performed using a laser power of approximately 200 μW, an 1800 lines mm^{-1} grating, and a $100\times$ objective with a numerical aperture of 0.95. Each spectrum was obtained by averaging a line scan comprising 20 points, with an integration time of 3 s per point. The positions and shapes of the characteristic E^1_{2g} and A_{1g} modes were analysed to compare the vibrational response of pristine and Nb-doped MoS_2.

After baseline subtraction, the E^1_{2g} and A_{1g} modes were fitted using pseudo-Voigt line profiles, with the same fitting range and fitting procedure applied to both samples. The peak positions, full widths at half maximum, and integrated areas were extracted from the fitted profiles.

Results and Discussion

The LEED patterns of pristine and Nb-doped MoS_2 recorded at a primary electron-beam energy of 93 eV are presented in Figure 1. The pristine sample exhibits a well-defined hexagonal diffraction pattern characteristic of an ordered MoS_2 surface. The Nb-doped sample also displays clearly resolved reflections arranged with hexagonal symmetry, indicating that long-range surface order is

retained after doping. However, the doped sample exhibits a more pronounced diffuse background and additional weak diffraction spots. These features may be associated with increased structural disorder, surface inhomogeneity, or the presence of additional surface domains. Their origin cannot be determined unambiguously from the LEED data alone.

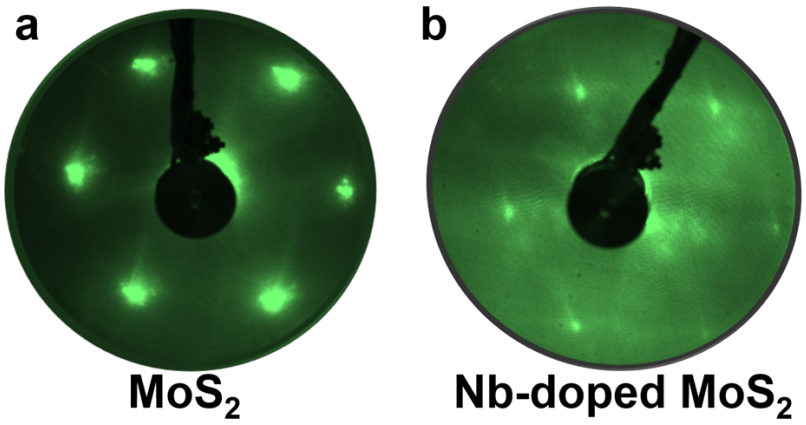

Figure 1. LEED patterns of (a) pristine and (b) Nb-doped MoS_2 recorded at a primary electron-beam energy of 93 eV. Both samples retain hexagonal surface order. The Nb-doped sample exhibits a more pronounced diffuse background and additional weak diffraction spots, indicating increased surface disorder or the presence of additional domains.

X-ray photoelectron spectroscopy was used to examine the surface elemental composition and electronic states of pristine and nominally 1% Nb-doped MoS_2. Because the samples were synthesized and analyzed in situ under vacuum conditions, exposure to ambient contaminants and oxygen was minimized.

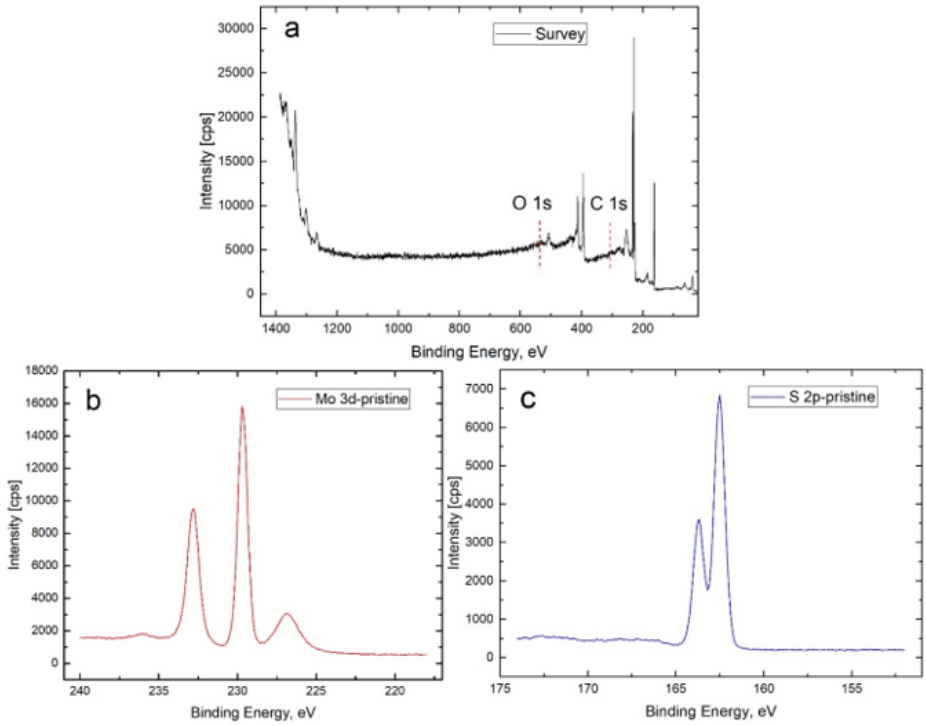

Figure 2. XPS characterization of pristine MoS_2 : (a) survey spectrum dominated by the characteristic Mo and S signals, with no clearly resolved C 1s or O 1s contributions; (b) high-resolution Mo 3d/S 2s spectrum showing the Mo 3d spin–orbit doublet and the S 2s contribution; and (c) high-resolution S 2p spectrum dominated by the sulfide S $2p_{3/2}$ –S $2p_{1/2}$ doublet.

The survey XPS spectrum of pristine MoS_2 is dominated by the characteristic Mo and S photoelectron signals, confirming that MoS_2 is the principal component of the analyzed surface. No clearly resolved C 1s or O 1s peaks are observed above the spectral background. This indicates that carbonaceous contamination and oxygen-containing surface species are negligible within the detection limit of the measurements, consistent with the in-situ preparation and XPS analysis under vacuum conditions.

The high-resolution Mo 3d/S 2s spectrum displays the characteristic Mo $3d_{5/2}$–Mo $3d_{3/2}$ spin–orbit doublet associated with Mo^{4+} in the Mo–S coordination environment. The additional feature at approximately 226 eV is assigned to the S 2s photoelectron line. The S 2p spectrum is dominated by the S $2p_{3/2}$–S $2p_{1/2}$ doublet characteristic of sulfide sulfur in the MoS_2 lattice. No pronounced high-binding-energy components are observed in either the Mo 3d or S 2p regions. Therefore, the presented spectra do not provide evidence of substantial surface oxidation or the formation of secondary sulfur-containing species. These assignments are consistent with established XPS characteristics of MoS_2.

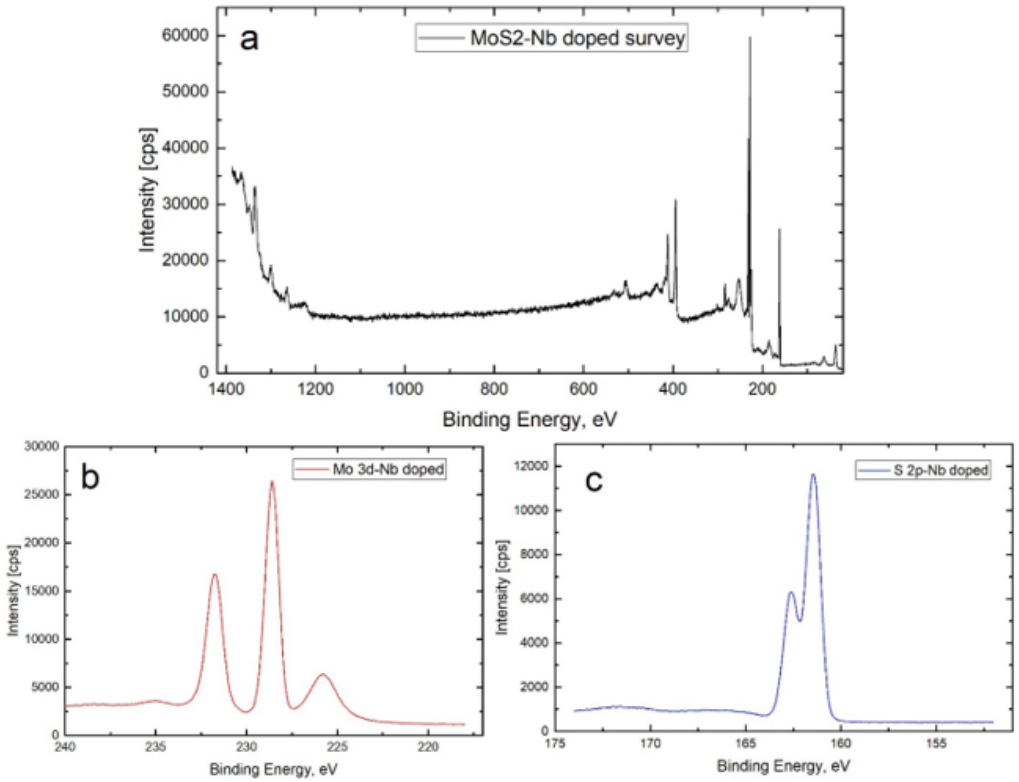

Figure 3. XPS characterization of nominally 1% Nb-doped MoS_2 : (a) survey spectrum dominated by Mo and S contributions; (b) high-resolution Mo 3d/S 2s spectrum showing the characteristic Mo 3d doublet and the S 2s contribution; and (c) high-resolution S 2p spectrum dominated by the sulfide S $2p_{3/2}$ –S $2p_{1/2}$ doublet. No statistically reliable Nb-related signal was resolved under the employed measurement conditions.

The survey spectrum of the nominally 1% Nb-doped sample retains the principal Mo and S features observed for pristine MoS_2, Figure 3. No additional intense signals attributable to secondary phases or substantial surface contamination are evident. This indicates that the MoS_2 matrix remains the dominant chemical component in the commercially supplied Nb-doped sample.

The high-resolution Mo 3d/S 2s spectrum of the Nb-doped sample contains

the characteristic Mo $3d_{5/2}$–Mo $3d_{3/2}$ doublet together with the S 2s contribution. Similarly, the S 2p region remains dominated by the sulfide S $2p_{3/2}$–S $2p_{1/2}$ doublet. The preservation of these spectral profiles indicates that the predominant Mo^{4+}–S^{2-} chemical environment of MoS_2 is maintained after nominal Nb doping. No clearly resolved additional components that could be assigned to substantial Mo or S oxidation are apparent in the raw spectra.

No statistically reliable Nb 3d doublet is resolved in the survey or high-resolution spectra. The nominal Nb concentration is only approximately 1%, and under the employed acquisition conditions the corresponding Nb signal may be too weak for reliable identification and quantification. The actual concentration within the surface-sensitive XPS sampling depth may also differ from the nominal synthesis composition because of incomplete incorporation or spatially nonuniform dopant distribution.

Therefore, the absence of a detectable Nb signal does not demonstrate that Nb is absent from the material. However, it means that the present XPS data cannot directly determine the Nb concentration, oxidation state, or lattice position. The sample should consequently be described as nominally 1% Nb-doped MoS_2, rather than as XPS-confirmed substitutionally doped MoS_2.

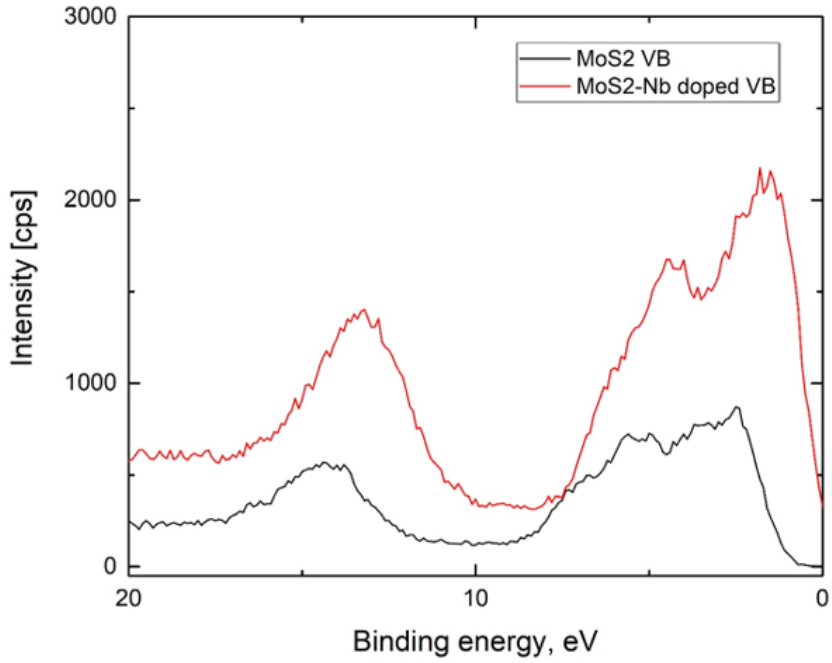

Figure 4. Valence-band and shallow-core-level XPS spectra of pristine and nominally 1 at.% Nb-doped MoS_2 over the 0–20 eV binding-energy range. The region below approximately 10 eV is predominantly associated with hybridized Mo 4d and S 3p valence states, whereas the feature at approximately 13–15 eV is mainly attributed to S 3s states. The spectra are presented without intensity normalization.

Figure 4 compares the valence-band XPS spectra of pristine and nominally 1 at.% Nb-doped MoS_2. The two samples exhibit similar overall spectral profiles, indicating that the principal electronic structure of the MoS_2 host matrix is preserved after nominal Nb doping. The difference in absolute spectral intensity is not interpreted quantitatively because the spectra were not intensity-normalized.

For quantitative comparison, the valence-band maximum was determined by linear extrapolation of the low-binding-energy leading edge to its intersection

with the fitted spectral background. The same fitting and energy-referencing procedure was applied to both samples. The $E_F - E_{VBM}$ separation decreased from approximately 0.9 eV for pristine MoS_2 to approximately 0.1 eV for nominally 1 at.% Nb-doped MoS_2. This corresponds to a shift of the valence-band maximum toward the Fermi level by approximately 0.8 eV.

The decrease in $E_F - E_{VBM}$ indicates that the Fermi level is located substantially closer to the valence-band maximum in the nominally Nb-doped sample. This behavior is consistent with an acceptor-type electronic modification associated with nominal Nb doping of MoS_2 [32].

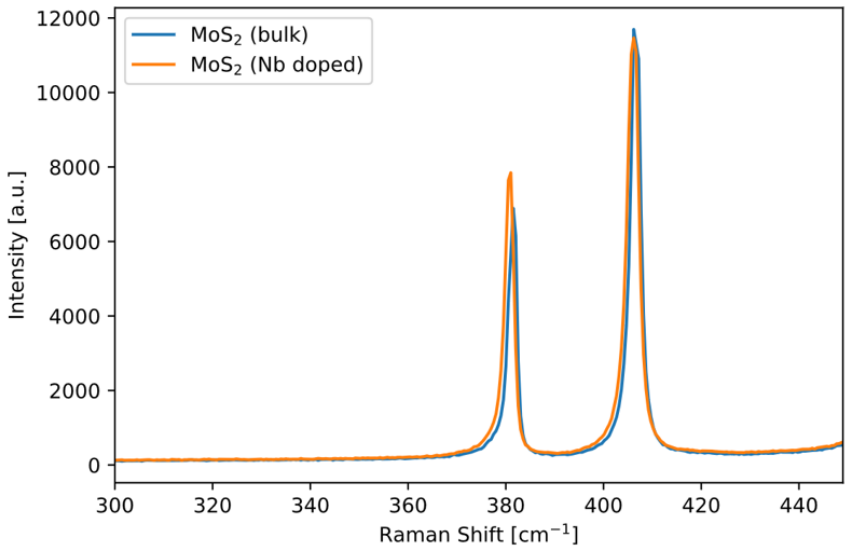

Figure 5. Raman spectra of pristine and nominally 1 at.% Nb-doped MoS_2. Both spectra exhibit the characteristic E^1_{2g} and A_{1g} modes of 2H- MoS_2, indicating preservation of the principal vibrational and layered structure of the MoS_2 host after nominal Nb doping.

The Raman spectra of pristine and nominally 1 at.% Nb-doped MoS_2 are presented in Figure 5. After baseline subtraction, the E^1_{2g} and A_{1g} modes were fitted using pseudo-Voigt line profiles, with the same fitting procedure applied to both samples. The fitted peak positions, full widths at half maximum, and relative integrated intensities are summarized in Table 1.

For pristine MoS_2, the E^1_{2g} and A_{1g} modes were centered at 381.43 and 406.64 cm^{-1}, respectively. In nominally Nb-doped MoS_2, these modes were observed at 380.70 and 406.05 cm^{-1}. Thus, the E^1_{2g} and A_{1g} modes exhibited red shifts of approximately 0.73 and 0.59 cm^{-1}, respectively.

The FWHM of the E^1_{2g} mode increased from 2.15 cm^{-1} in pristine MoS_2 to 2.35 cm^{-1} in nominally Nb-doped MoS_2. The FWHM of the A_{1g} mode increased from 2.73 to 2.96 cm^{-1}. The fitted A_{1g}/E^1_{2g} integrated-area ratio decreased from approximately 2.26 to 2.08. Meanwhile, the separation between the two modes changed only slightly, from 25.21 to 25.36 cm^{-1}. The mode separation therefore remained approximately 25 cm^{-1}, confirming retention of the characteristic bulk 2H- MoS_2 vibrational structure.

Table 1.
Quantitative Raman fitting results.

Parameter	Pristine MoS_2	Nominally Nb-doped MoS_2	Change
E^1_{2g} peak position (cm^{-1})	381.43	380.70	-0.73
A_{1g} peak position (cm^{-1})	406.64	406.05	-0.59
FWHM of E^1_{2g} (cm^{-1})	2.15	2.35	$+0.20$
FWHM of A_{1g} (cm^{-1})	2.73	2.96	$+0.23$
A_{1g}/E^1_{2g} integrated-area ratio	2.26	2.08	-0.18
Mode separation (cm^{-1})	25.21	25.36	$+0.15$

The small red shifts, modest linewidth broadening, and limited change in the relative integrated intensity indicate a measurable but relatively weak perturbation of the MoS_2 lattice in the nominally Nb-doped sample. These changes are compatible with local strain, structural disorder, and possible charge redistribution. The modest broadening is also consistent with the enhanced diffuse background observed in the LEED pattern of the nominally Nb-doped sample, which independently indicates a higher degree of structural disorder or surface inhomogeneity.

Conclusion

The combined LEED, XPS, and Raman spectroscopy results demonstrate that Nb-doped MoS_2 retains the principal structural, chemical, and vibrational characteristics of the parent 2H-MoS_2 matrix. LEED confirms the preservation of hexagonal surface order, although the enhanced diffuse background indicates an increased degree of structural disorder. XPS results show that the nominally 1 at.% Nb-doped sample retains the principal Mo^{4+}–S^{2-} chemical environment and the characteristic electronic structure of the MoS_2 host matrix. No substantial surface contamination, oxidation, or secondary sulfur-containing phase is evident. Although the Nb 3d signal was not directly resolved because of the low nominal dopant concentration, the correlated shift of the valence-band, Mo 3d, and S 2p features toward lower binding energy provides indirect evidence of an Nb-induced modification of the electronic structure, consistent with acceptor-type Nb incorporation into MoS_2. The Raman spectra retain the characteristic E^1_{2g} and A_{1g} modes, indicating the absence of any large-scale phase transformation following doping. Thus, low-level Nb doping modifies the local structural and chemical environment without disrupting the overall MoS_2 structure.

Acknowledgement

This work was supported by the Science Committee of the Ministry of Science and Higher Education of the Republic of Kazakhstan (Grant No. AP26197187).

References

[1] K.S. Novoselov et al., Nature **438** (2005) 197–200. [*CrossRef*]
[2] K.S. Novoselov et al., Science **306** (2004) 666–669. [*CrossRef*]
[3] Y. Chen et al., Nature Physics **16** (2020) 218–224. [*CrossRef*]
[4] C. Rubio-Verdu et al., Nano Letters **20** (2020) 5111–5118. [*CrossRef*]
[5] S. Goswami, S. Goswami, T. Venkatesan, Applied Physics Reviews **7** (2020) 021303. [*CrossRef*]
[6] S.Z. Butler et al., ACS Nano **7** (2013) 2898–2926. [*CrossRef*]
[7] C.-P. Lu et al., Nano Letters **14** (2014) 4628–4633. [*CrossRef*]
[8] S. Shree et al., 2D Materials **7** (2020) 015011. [*CrossRef*]
[9] Y.-H. Lee et al., Advanced Materials **24** (2012) 2320–2325. [*CrossRef*]
[10] K.F. Mak et al., Physical Review Letters **105** (2010) 136805. [*CrossRef*]
[11] Q. Tang, D. Jiang, Chemistry of Materials **27** (2015) 3743–3748. [*CrossRef*]
[12] M. Chen et al., ACS Nano **8** (2014) 4023–4032. [*CrossRef*]
[13] M. Timpel et al., npj 2D Materials and Applications **5** (2021) 64. [*CrossRef*]
[14] G. Li et al., Journal of the American Chemical Society **138** (2016) 16632–16638. [*CrossRef*]
[15] M. Moun et al., Scientific Reports **8** (2018) 11799. [*CrossRef*]
[16] X. Huang et al., Advanced Materials **26** (2014) 2185–2204. [*CrossRef*]
[17] S. Manzeli et al., Nature Reviews Materials **2** (2017) 17033. [*CrossRef*]
[18] D.J. Trainer et al., npj 2D Materials and Applications **6** (2022) 13. [*CrossRef*]
[19] J. Hong et al., Nature Communications **6** (2015) 6293. [*CrossRef*]
[20] K. Zhussupbekov et al., Advanced Science **12** (2025) e04394. [*CrossRef*]
[21] Q. Liang et al., ACS Nano **15** (2021) 2165–2181. [*CrossRef*]
[22] B. Schuler et al., Physical Review Letters **123** (2019) 076801. [*CrossRef*]
[23] Z. He et al., ACS Applied Materials & Interfaces **10** (2018) 42524–42533. [*CrossRef*]
[24] K. Zhussupbekov et al., npj 2D Materials and Applications **5** (2021) 14. [*CrossRef*]
[25] P. Huang et al., npj 2D Materials and Applications **7** (2023) 6. [*CrossRef*]
[26] X. Liu et al., Nano Letters **21** (2021) 4887–4893. [*CrossRef*]
[27] S. Barja et al., Nature Communications **10** (2019) 3382. [*CrossRef*]
[28] D. Edelberg et al., Nano Letters **19** (2019) 4371–4379. [*CrossRef*]
[29] S. Zhang et al., Physical Review Letters **119** (2017) 046101. [*CrossRef*]
[30] K. Ko et al., Journal of Applied Physics **135** (2024) 100901. [*CrossRef*]
[31] D.-H. Yang et al., Materials Horizons **11** (2024) 747–757. [*CrossRef*]
[32] J. Suh et al., Nano Letters **14** (2014) 6976–6982. [*CrossRef*]